SEMARAK ILMU PUBLISHING

Journal of Advanced Research in Fluid Mechanics and Thermal Sciences

Journal homepage:
https://semarakilmu.com.my/journals/index.php/fluid_mechanics_thermal_sciences/index
ISSN: 2289-7879

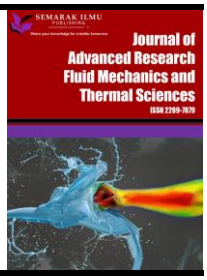

Effect of Magnetic Field on the Developing Thermal Field in a Duct Filled with Porous Media under Local Thermal Non-Equilibrium with a Nonlinear Flow Model

Nitish Gupta[1], Devarakonda Bhargavi[1,*]

[1] Department of Mathematics, National Institute of Technology, Warangal, 506004, India

ARTICLE INFO

Article history:
Received 30 August 2022
Received in revised form 10 January 2023
Accepted 17 January 2023
Available online 4 February 2023

Keywords:
Local thermal non-equilibrium model; Darcy Brinkman Forchheimer model; Hartmann number; porous medium; wall heat flux

ABSTRACT

In this article, the numerical study of the influence of a magnetic field at the laminar forced convection in a thermally developing region coming under the influence of local thermal non-equilibrium (LTNE) of parallel plate channels completely immersed in the porous material is investigated. Constant wall heat flux boundary conditions are applied to the walls of the channel. In the nonlinear flow model, the Darcy-Brinkman-Forchheimer equation governs the flow field in the porous region, which is assumed to be unidirectional. The system is defined by certain well-known parameters, these being Darcy number (*Da*), thermal conductivity ratio (κ), Forchheimer number (*F*), Hartmann number (*M*), and Biot number (*Bi*). Numerical solutions have been obtained by applying a successive accelerated replacement (SAR) scheme. Exact solutions for the dimensionless temperature and the fully developed Nusselt number in the absence of the Forchheimer number ($F = 0$), for the fully developed thermal field, are obtained for the linear flow model, the Darcy-Brinkman model. Plots are given for the dimensionless temperature profiles in the fluid and solid phases, wall temperature, as well as the local Nusselt number at the parallel plate channel, which has been displayed. The effect of the magnetic field and the thermal conductivity ratio has a significant effect on the local Nusselt number.

1. Introduction

Numerous theoretical and experimental studies have recently been carried out in various fields based on fluid flow and convection heat transmissions in porous media, which have gotten a lot of attention in recent decades due to their many engineering applications, such as heat pipes, gas and water management in fuel cells, petroleum reservoirs, water, and solute transport in building materials, solar power collectors, textiles, nuclear reactors, drying of paper pulp, compact heat exchangers, and Microfluidic paper-based analytical devices [1]. The fundamental transport phenomena in porous media have since been thoroughly studied using a local thermal equilibrium (LTE) model, which disregards the temperature difference between the solid and fluid phases. Significant research on convective transport in porous media has been carried out under the

* *Corresponding author.*
E-mail address: bhargavi@nitw.ac.in

https://doi.org/10.37934/arfmts.103.1.87104

assumption that the fluid and solid-matrix phases are in LTE. Vafai and Tien [2] demonstrated this first, and it was later reviewed in monographs by Nield and Bejan [3] and Nakayama [4]. This LTE hypothesis, however, frequently fails for practical engineering problems, as noted by Amiri and Vafai [5], and Carbonnel and Whitaker [6]. As an alternative to the LTE model, Nield and Bejan [3] discussed the local thermal non-equilibrium (LTNE) model, which allows temperature difference between solid and fluid phases with interphase temperature difference.

Many researchers have shown a keen interest in these issues. It might be because there are so many fascinating and limitless ways to use these equations in real-time applications such as the upkeep of reactors generating nuclear power [7]; in flows that assume nanofluid order [8, 9]; in flows in metallic foams [10]; liquid nitrogen jet fracturing for HDR reservoirs [11], and bioheat transfer [12]. The effects of LTNE on the beginning of convection in a vertical throughflow internally heated layered porous medium were examined by Kuznetsov and Nield [13]. With linear and nonlinear flow models, Yi *et al.,* [14, 15] investigated the LTNE effect for parallel plate geometry. Lee and Vafai [16], Amiri *et al.,* [17] and Marafie and Vafai [18], completed a thorough investigation into the effects of using different boundary conditions under LTNE conditions. Unsteady heat transfer has been studied by Singh *et al.,* [19] under LTE and LTNE in a porous medium contained in a tube. However, for multi-layered micro-heat exchangers in a porous medium with the flow and thermal slip conditions, the effects of LTNE on the beginning of convection in a vertical throughflow internally heated layered porous medium were examined by Kuznetsov and Nield [13].

Magnetohydrodynamic (MHD) flow and heat transfer above a plate for a viscous incompressible fluid has a wide range of uses in engineering and business, including spacecraft power generation, hypersonic wind tunnel experiments, laser power MHD generators, plasma studies, defense sectors, and petroleum industries among others. The flow of electric current through a magnetic field and body force affects the Lorentz force. Numerous researchers, including Sreekala and Reddy [20], Kiema *et al.*, [21], Chauhan and Rastogi [22], and Onyango *et al.*, [23] investigated two-dimensional MHD flow and heat transfer through channels and plates with various boundary conditions. When viscosity dissipation and Joule heating are present, Raju *et al.*, [24] examined the MHD-driven convective flow of a viscous fluid. The effect of magnetic fields on fluid flow has been studied by several authors (Vineet Kumar and Amit Kumar [25], Kurzweg [26], and Raptis and Kafousias [27]) using a variety of scenarios and various geometries. Bhargavi and Sharath Kumar Reddy [28] investigated the impact of the magnetic field on the Brinkman extended non-Darcy flow model. The boundary layer flow in a porous region was studied by Pal [29] using Darcy Brinkman Forchheimer's model. The magnetic field has been found to have a significant impact on boundary layer velocity.

The analysis in the present work is based on temperature distribution, wall temperatures in the fluid and solid phases, and variations in the local Nusselt number in porous media. The nonlinear flow model, the Darcy-Brinkman-Forchheimer equation governs the flow field in the porous region, which is assumed to be unidirectional. For constant flux wall boundary conditions, as far as the author is aware, the effect of the Hartman number on wall temperatures at the channel's entry in both phases is not discussed. Numerical solutions have been obtained by applying a successive accelerated replacement (SAR) scheme. Exact solutions for the dimensionless temperature and the fully developed Nusselt number in the absence of the Forchheimer number ($F = 0$), for the fully developed thermal field, are obtained for the linear flow model, the Darcy-Brinkman model. Plots are given for the dimensionless temperature profiles in the fluid and solid phases, wall temperature, as well as the local Nusselt number at the parallel plate channel, which has been displayed. The effect of the magnetic field and the thermal conductivity ratio has a significant effect on the local Nusselt number.

2. Mathematical Model and Boundary Conditions

The schematic model and coordinate system of the parallel plate channel are shown in Figure 1. The distance between the parallel plates is denoted by H, and T_e the fluid enters the channel at a uniform temperature (Figure 1). The constant wall heat flux (q_w) has been applied to channel walls. The following assumptions are considered in the present analysis

i. The Darcy Brinkman Forchheimer model for the fluid flow through the porous region.
ii. The flow is laminar, incompressible, steady, and unidirectional.
iii. The magnetic field, B_o is applied transversely along the channel walls.
iv. Porous and fluid regions are in LTNE.
v. The flow field is fully developed hence dp/dx^* is a constant and developing thermal field.
vi. Heat generation, axial conduction, and thermal dispersion are negligible.
vii. The porous medium is isotropic and homogeneous.
viii. The thermophysical properties are constant.

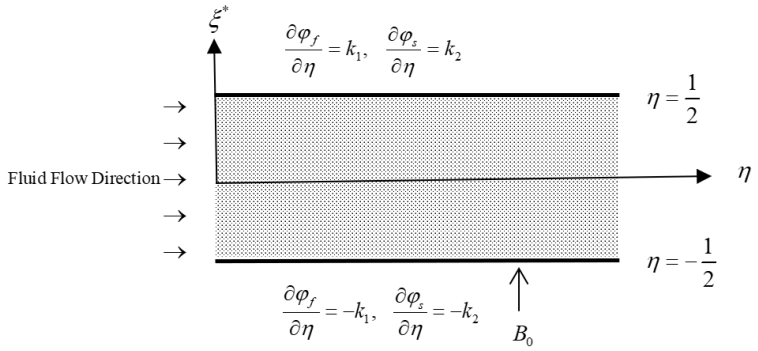

Fig. 1. Schematic model and coordinate system

2.1 Governing Equations

The dimensionless variables specified below are used to establish the governing equations dimensionless.

$$\left.\begin{aligned} &\xi = x^* / H,\ \eta = y^* / H,\ U = u / u_{ref},\ U_p = \frac{u_p \mu}{\left(-dp/dx^*\right)H^2},\ U_{avg} = \frac{u_{avg}\mu}{\left(-dp/dx^*\right)H^2}, \\ &\varphi_f = \frac{\left(T_f - T_e\right)}{\left(q_w H / k_f\right)},\ \varphi_s = \frac{\left(T_s - T_e\right)}{\left(q_w H / k_f\right)} \end{aligned}\right\} \quad (1)$$

In Eq. (1), ξ and η are the dimensionless coordinates. The dimensionless temperature and velocity are denoted by φ and U, respectively. The fluid and solid phases are designated by subscripts f and s, respectively. The average velocity across the channel is denoted by u_{avg}. The Peclet number (Pe) can be absorbed and defined in Eq. (2), at the condition, when the channel walls are exposed to a continuous heat flow.

$$\xi^* = \xi / Pe \quad (2)$$

In Eq. (2), ξ^* is the normalized dimensionless axial distance. The dimensionless form of governing equations (after applying the dimensionless variables given by Eq. (1)).

$$\frac{1}{\varepsilon}\frac{d^2U_P}{d\eta^2}-\left(\frac{1}{Da}+M^2\right)U_P-F\ U_P{}^2+1=0 \tag{3}$$

$$U_p(\eta)\frac{\partial\varphi_f}{\partial\xi^*}=\frac{1}{k_1}\frac{\partial^2\varphi_f}{\partial\eta^2}+\frac{Bi\ \kappa}{k_1}\left(\varphi_s-\varphi_f\right) \tag{4}$$

$$\frac{\partial^2\varphi_s}{\partial\eta^2}-Bi\left(\varphi_s-\varphi_f\right)=0 \tag{5}$$

Eq. (3) is the dimensionless form of conservation of momentum equation [30,31], and Eq. (4) and (5) are the dimensionless form of thermal energy equations (LTNE model [13-15]).

In Eq. (3) to (5), *Da*, *M*, *F*, and *Bi* denote the Darcy number, Hartman number, Forchheimer number, and Biot number, respectively [32-37]; however, ε, k_1 and, κ represent the ratio between the viscosity of the fluid to the effective viscosity of the porous, fluid thermal conductivity to porous thermal conductivity, effective solid thermal conductivity to effective fluid thermal conductivity in the porous region, respectively and it can be defined as

$$Da=K/H^2 \tag{6}$$

$$M=\sqrt{\sigma B_0^2H^2/\mu_f} \tag{7}$$

$$F=\rho C_FH^4\left(-dp/dx^*\right)/\sqrt{K}\mu^2 \tag{8}$$

$$Bi=\left(a_{sf}h_{sf}H^2\right)/k_{se} \tag{9}$$

$$\varepsilon=\mu/\mu_{eff} \tag{10}$$

$$k_1=k_f/k_{fe} \tag{11}$$

$$\kappa=k_{se}/k_{fe} \tag{12}$$

2.2. Dimensionless Boundary Conditions

Hydrodynamics boundary condition

$$\left.\begin{aligned} U_p = 0, \quad \text{at} \quad \eta = \pm\frac{1}{2} \\ \frac{dU_p}{d\eta} = 0 \quad \text{at} \quad \eta = 0 \end{aligned}\right\} \tag{13}$$

Thermal boundary condition

$$\left.\begin{aligned} \frac{\partial \varphi_f}{\partial \eta} = k_1, \ \frac{\partial \varphi_s}{\partial \eta} = k_2 \qquad \text{at} \quad \eta = \frac{1}{2} \\ \frac{\partial \varphi_f}{\partial \eta} = -k_1, \ \frac{\partial \varphi_s}{\partial \eta} = -k_2 \quad \text{at} \quad \eta = -\frac{1}{2} \end{aligned}\right\} \tag{14}$$

where in Eq. (14), the ratio, k_2 is defined by

$$k_2 = k_f \,/\, k_{se} \tag{15}$$

$$\varphi_{f,s}(0,\eta) = 0, \quad \text{for} \ -\frac{1}{2} \le \eta \le \frac{1}{2} \tag{16}$$

Interface boundary condition

$$\varphi_f = \varphi_s = \varphi_{interface} \tag{17}$$

3. Local Nusselt Number

The local heat transfer coefficient (h_ξ) is determined at the wall $y^* = H/2$ adjacent to the porous medium as follows

$$-k_{fe}\left(\partial T_f / \partial y^*\right)_{y^*=H/2} = h_\xi \left(T_w - T_b\right) \tag{18}$$

In Eq. (18), the bulk mean temperature (T_b) is denoted as follows

$$T_b = \int_{-H/2}^{H/2} u_p T_f dy^* \Bigg/ \int_{-H/2}^{H/2} u_p dy^* \tag{19}$$

Upon dimensionless variables {using Eq. (1)}, the local Nusselt number at $\eta = 1/2,,$ Nu_ξ is given by

$$Nu_\xi = h_\xi (2H) k_1 / k_f = 2 \Big/ \left(\varphi^* - \varphi_w\right) \tag{20}$$

In Eq. (20), φ_w and φ^* are defined by

$$\varphi_w = \left(T_w - T_e\right) / \left(qH / k_f\right) \tag{21}$$

$$\varphi^* = \left(T_b - T_e\right) / \left(qH / k_f\right) \tag{22}$$

where φ^* is evaluated by

$$\varphi^* - \varphi_w\left(\xi^*\right) = \int_{-1/2}^{1/2} U_p\left(\varphi_f - \varphi_w\right) d\eta \Big/ \int_{-1/2}^{1/2} U_p d\eta \tag{23}$$

Dimensionless temperature based on bulk mean temperature, φ_b defined by

$$\varphi_b = \frac{T - T_e}{T_b - T_e} = \frac{\varphi}{\varphi^*} \tag{24}$$

4. Limiting Case

4.1 Case 1: F = 0.0, M ≠ 0.0

Analytical expressions for dimensionless temperature and the fully developed Nusselt number for Forchheimer number, *F* = 0.0 for the fully developed thermal field are given for the Darcy Brinkman Model [28]. Dimensionless form Darcy Brinkman model is given by

$$\frac{1}{\varepsilon}\frac{d^2U_P}{d\eta^2} - \left(\frac{1}{Da} + M^2\right)U_P + 1 = 0 \tag{25}$$

Solving the set of equations Eq. (3), (4), and (25) along with boundary conditions Eq. (13) and (14). The temperature profiles in the fluid and solid phases are expressed relative to φ_{wf}, and φ_{ws} respectively.

For the Darcy Brinkman model, the dimensionless temperature in the fluid and solid phases, as well as the fully developed Nusselt number expressions, are given by

4.2 Darcy Brinkman Model

The dimensionless temperature in fluid and solid phases

$$\theta_{wf} - \theta_f(\eta) = \frac{\lambda k_1 \left\{ \begin{array}{l} 2A_2^4 \left\{ e^{\frac{\sqrt{\kappa Bi}(1-2\eta)}{\sqrt{2}}} + e^{\frac{\sqrt{\kappa Bi}(1+2\eta)}{\sqrt{2}}} - e^{\sqrt{2\kappa Bi}} - 1 \right\} + \kappa Bi A_2^2 A_3 \left[\kappa Bi\left(1-4\eta^2\right)\left(1-A_2^2\right) + 8 \right] \\ +8\kappa Bi A_3 \left[A_4 A_5 \cosh\left[\eta A_2\right] - \kappa Bi \right] \end{array} \right\}}{8\kappa Bi A_2 A_3 A_4 A_7} \tag{26}$$

$$\theta_{ws}-\theta_s(\eta)=-\frac{\lambda k_1 e^{\sqrt{\frac{\kappa Bi}{2}}}\left\{A_5\cosh\left[\sqrt{\frac{\kappa Bi}{2}}\right]\left\{\begin{matrix}A_4\cosh\left[\frac{A_2}{2}\right]\left\{\begin{matrix}4A_2{}^2+8\kappa Bi\\+\kappa Bi\left(4\eta^2-1\right)A_2{}^2\end{matrix}\right\}\\-16\kappa^2 Bi^2\cosh\left[\eta A_2\right]\end{matrix}\right\}+4A_2{}^4\cosh\left[\sqrt{2\kappa Bi}\eta\right]\right\}}{8\kappa Bi\left(2\kappa Bi-A_2{}^2\right)A_2A_3A_7} \tag{27}$$

In Eq. (26) and (27), dimensionless wall temperatures in fluid and solid phases, φ_{wf}, and φ_{ws} are defined by

$$\varphi_{wf}=\left(T_{wf}-T_e\right)/q_wH/k_f\,,\quad \varphi_{ws}=\left(T_{ws}-T_e\right)/q_wH/k_f \tag{28}$$

4.3 Fully Developed Nusselt Number (Nu_{fd})

The constants, A_i, i = 1,2,3, …, 14, 15, appearing in Eq. (26), (27), and (29) are given in Appendix. The variation of fully developed Nusselt number, Nu_{fd} with *Bi* is shown in Figure 2(a)-(c) for various thermal conductivity ratios κ = 0.1, 1.0, and 10.0 respectively for Hartman numbers, *M* = 1, 3, 5, 8 and, 10. Nu_{fd} rises to certain *Bi* then, it decreases as *Bi* decreases for all the Hartman numbers and κ. For all the Biot number values, as the Hartman number increases, Nu_{fd} increases. Also, Nu_{fd} decreases as κ increases for a given *Bi*, *M*, and *Da.*

$$Nu_{fd}=\frac{\left\{12\kappa BiDa^2A_7\sqrt{\varepsilon A_1}A_{11}{}^2+\left\{\frac{4\sqrt{\kappa Bi}\left(-\kappa BiDa+\varepsilon A_1\right)A_{10}}{Da}-\frac{2e^{\sqrt{\frac{\kappa Bi}{2}}}\sqrt{\kappa A_1}A_{13}}{Da^{3/2}}\right\}\right\}}{\left\{-A_{11}\left\{\begin{matrix}-6\sqrt{2}\left(e^{\sqrt{2\kappa Bi}}-1\right)\varepsilon^{7/2}A_1{}^{7/2}\\+\frac{1}{A_6\sqrt{\kappa Bi}}\left\{\begin{matrix}\sqrt{\varepsilon A_1}A_3\left\{\begin{matrix}\left[\left(6+\kappa Bi\right)A_1\varepsilon-24\kappa BiDa\right]\cosh\left[A_2\right]A_9^2+A_{14}\\-4\kappa BiDa\left(18+\kappa Bi\right)\varepsilon^2A_1{}^2+\left(6+\kappa Bi\right)\varepsilon^3A_1{}^3\end{matrix}\right\}\\+12\kappa BiDa^{3/2}\left[2A_6A_{10}A_{15}+\kappa Bi\sqrt{\varepsilon DaA_1}\left(2e^{\sqrt{2\kappa Bi}}+A_6A_5^2\right)A_{12}\right]\end{matrix}\right\}\end{matrix}\right\}\right\}} \tag{29}$$

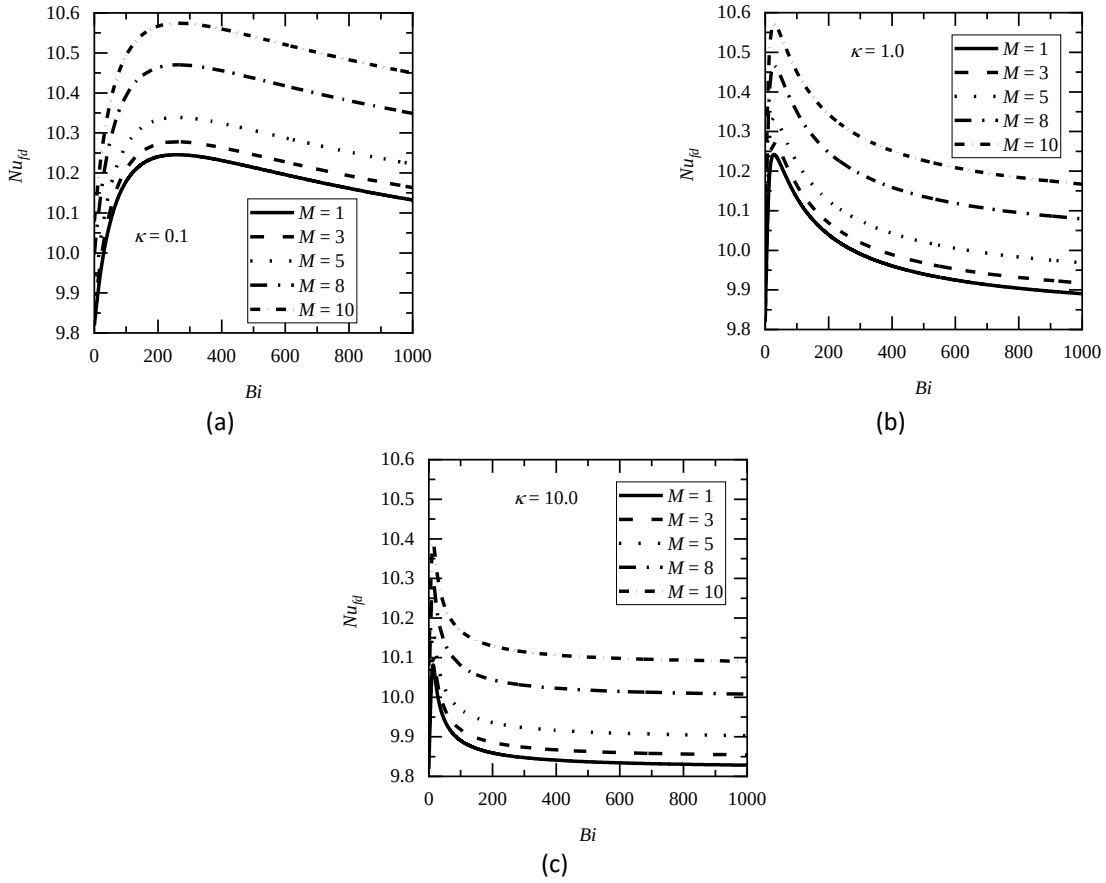

Fig. 2. Nu_{fd} variation with *Bi* for the Darcy Brinkman model for (a) κ = 0.1, (b) κ = 1.0, and (c) κ = 10.0 at *Da* = 0.005 for distinct Hartmann numbers, *M*

4.4 Case 2: F ≠ 0.0, M = 0.0

In the absence of the Hartman number, *M* (*M* = 0), the velocity profiles are matching with the paper done by Sharath Kumar Reddy and Bhargavi [38], and Gupta and Bhargavi [39] for all the values of the Forchheimer number (*F*) and the channel filled with the porous material.

5. Numerical Methodology and Results and Discussion

The successive accelerated replacement (SAR) methodology has been widely used in the literature [38-40], to generate numerical solutions to Eq. (3) to (5) along with the boundary conditions (Eq. (13), (14), and (16)). 0.001 ≤ *Da* ≤ 0.1, 1 ≤ *Bi* ≤ 100, 1 ≤ *F* ≤ 100, 1 ≤ *M* ≤ 65, and 0.1 ≤ κ ≤ 10 are the ranges used for parameters. It is assumed that $k_1 = k_f / k_{fe} = 1$, $k_2 = k_f / k_{se} = 1$, and $\varepsilon = \mu / \mu_{eff} = 1$

5.1 Hydrodynamics

In this section, the velocity profiles for flow through a channel filled with porous material have been investigated.

5.1.1 Velocity profile

Figure 3 and 4 illustrate the dimensionless velocity profiles at distinct values of Hartman number (*M*) and at *Da* = 0.01, and *Da* = 0.1 for Forchheimer numbers *F* = 1 and 100, respectively. It may be remarked that the value of dimensionless velocity U_p decreases with the increment in *M* for all Forchheimer numbers (*F*). The decrease in the velocity is expected due to a rise in the Hartman number. However, it is also clear from these figures that for all the Hartman numbers, the dimensionless velocity U_p rises as the Forchheimer number (*F*) increases. By comparing Figure 3 and 4, it is clear that as Darcy number increases, U_p also increases and for a large value of *Da,* the increase in the velocity is more because for large *Da* the porous region begins to behave like a clear fluid region. These velocity profiles match those reported in Sharath Kumar Reddy and Bhargavi [38] for channel filled porous region and in the absence of Hartman number (*M* = 0).

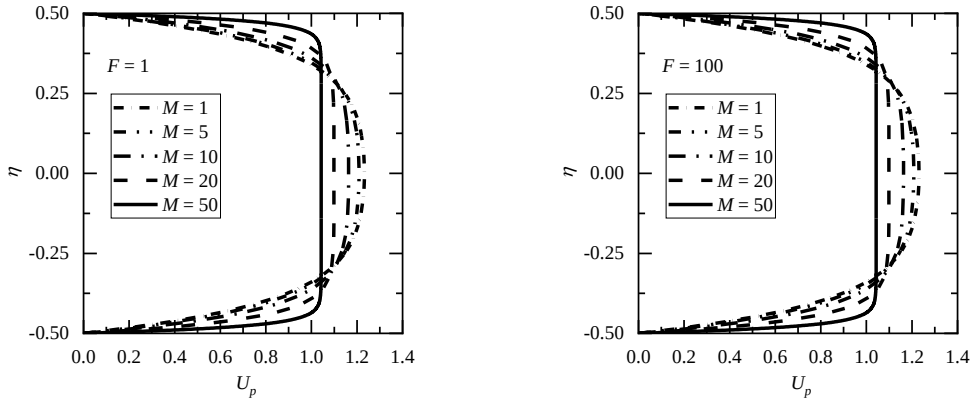

(a) (b)

Fig. 3. Effect of U_p for distinct *M* values at (a) *F* = 1, and (b) *F* = 100 for *Da* = 0.01

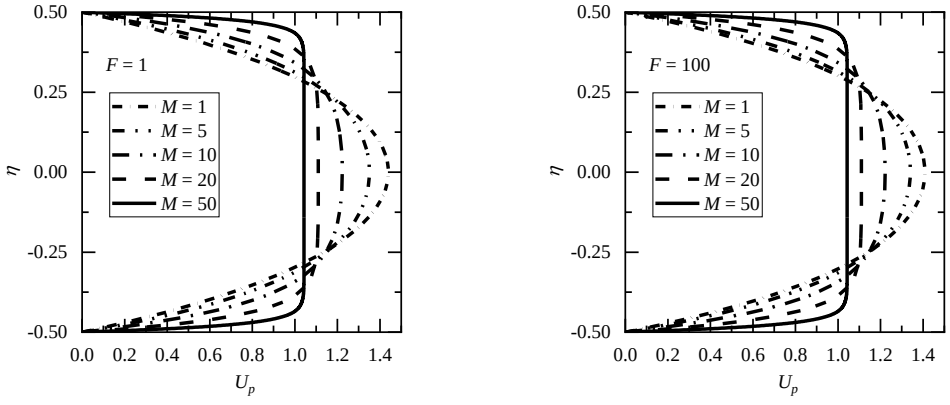

(a) (b)

Fig. 4. Effect of U_p for distinct *M* values at (a) *F* = 1, and (b) *F* = 100 for *Da* = 0.1

5.2 Thermal Field

The dimensionless temperature profiles and the wall temperatures in both phases solid and fluid as well as the local Nusselt number for flow through the porous filled channel are examined in the present section.

5.2.1 Dimensionless temperature in the fluid phase and solid phase

Dimensionless temperature profiles, φ_f in fluid phase for Biot numbers *Bi* = 10, Forchheimer number *F* = 10, *Da* = 0.001, and κ = 0.1 at different values of ξ^* are shown in Figure 5 for Hartman numbers, (a) *M* = 1, and (b) 65 respectively. A similar type of plot is given for φ_s in the solid phase in Figure 6. Dimensionless temperature profiles (a) φ_f and (b) φ_s for *Bi* = 100, *F* = 10, *Da* = 0.001, and κ = 0.1 at different values of ξ^* are shown in Figure 7 for *M* = 1. A similar type of plot is shown in Figure 8 for *Bi* = 10.0 and κ = 10.0

Since the channel is symmetric, it can be observed from Figures 5 to 8, wall temperatures $\varphi_{wf}\big|_{\eta=+1/2} = \varphi_{wf}\big|_{\eta=-1/2}$ and $\varphi_{ws}\big|_{\eta=+1/2} = \varphi_{ws}\big|_{\eta=-1/2}$. This observation can be seen in Gupta and D. Bhargavi [39]. φ_f and φ_s profiles are symmetric about $\eta = 0$.

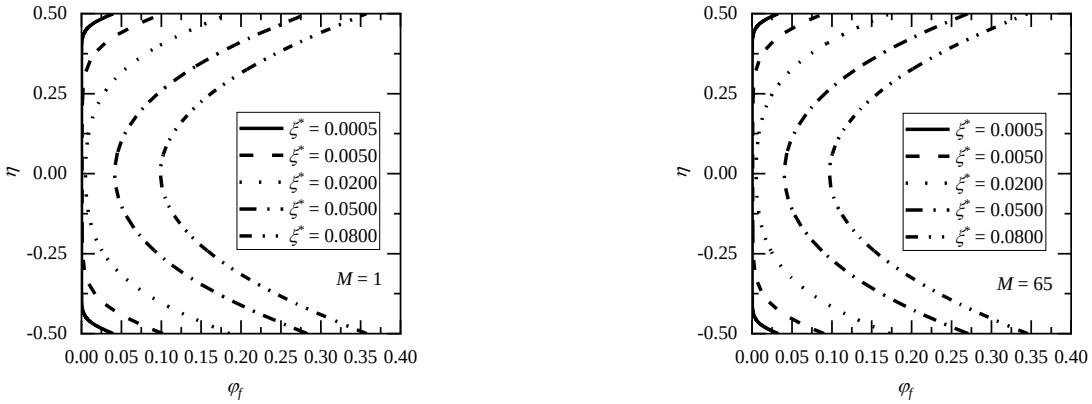

Fig. 5. Impact of φ_f for distinct ξ^* for *Bi* = 10 and κ = 0.1 at *Da* = 0.001 for (a) *M* = 1 and (b) *M* = 65

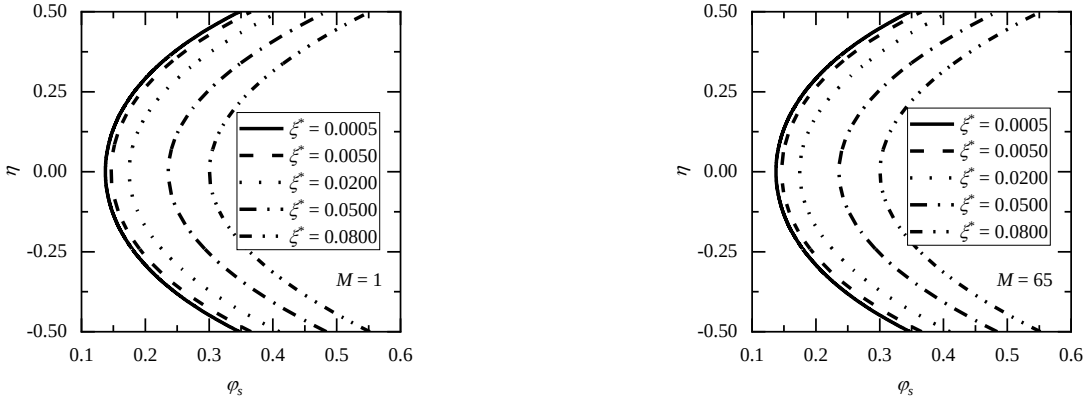

Fig. 6. Impact of φ_s for distinct ξ^* values for *Bi* = 10 and κ = 0.1 at *Da* = 0.001 for (a) *M* = 1 and (b) *M* = 65

From Figure 5 and 6, It is observed that for all Hartman numbers (*M*) and Forchheimer numbers (*F*), φ_f, and φ_s increase with an increase of ξ^*. Moreover, as Hartman number (*M*) increases, φ_f, and φ_s decreases for all the values of ξ^*. By comparing of Figure 5(a) and Figure 7(a) and Figure 6(a)

and Figure 7(b), as *Bi* increases from 10 to 100, it can be seen that there is a less increment in φ_f, whereas φ_s is decreasing and tends to temperature in a fluid region under LTE. It means LTNE tends to LTE when the Biot number is large. This is happening for all the values of the Hartman number, Forchheimer number, and Darcy number.

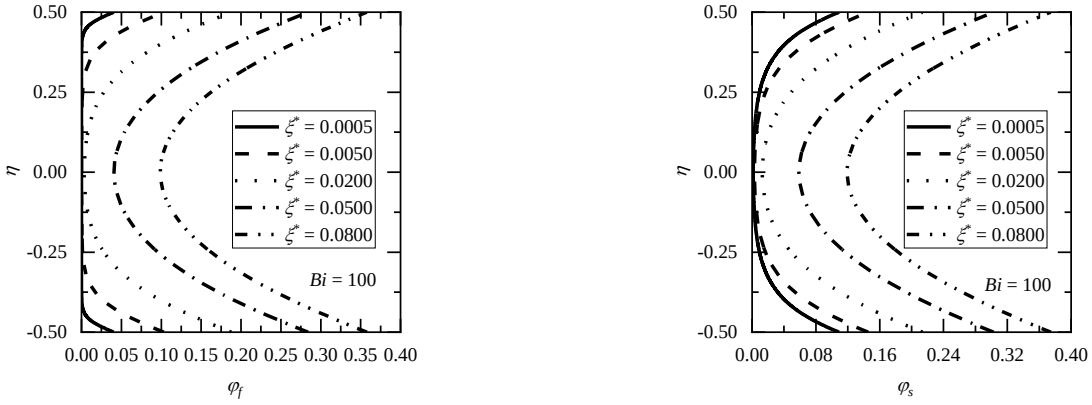

(a) (b)

Fig. 7. Impact of (a) φ_f, and (b) φ_s for distinct ξ^* values at the high Biot number, *Bi* = 100 for κ = 0.1, *Da* = 0.001 and, *M* = 1

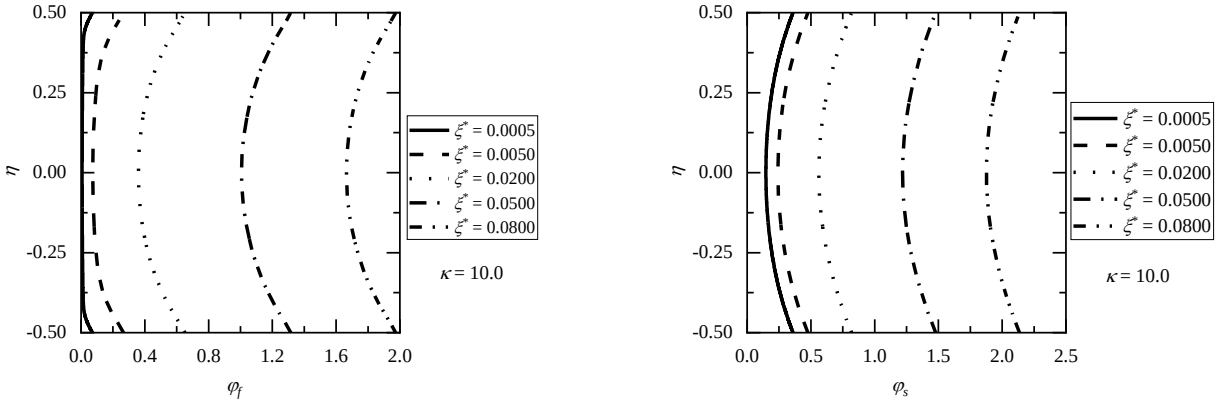

(a) (b)

Fig. 8. Impact of (a) φ_f, and (b) φ_s for distinct ξ^* values at the large value of κ = 10.0 for *F* = 10, *Bi* = 10, *Da* = 0.001 and, *M* = 1

By comparing Figure 5(a), Figure 8(a) and, Figure 6(a) Figure 8(b) as the thermal conductivity ratio, $\kappa\left(=k_{se}/k_{fe}\right)$ increases, φ_f, and φ_s increase, it is due to increases in the effective thermal conductivity of the fluid, k_{fe}. From Figure 5 to 8, it can also be observed that temperature in a solid phase, φ_s is larger than the temperature in a fluid phase φ_f. This is due to the LTNE condition. There is very less effect of the Forchheimer number on φ. Hence plots are given for *F* = 10 only.

5.2.2 Wall temperature

Since the constant heat flux conditions at the walls are applied, wall temperatures will not be known. Hence to see the effect of the relevant parameters, wall temperature profiles are given. The variations of wall temperatures in fluid phase (φ_{wf}) and solid phase (φ_{ws}) with ξ^* for *F* = 100, *Bi* = 10,

and κ = 1.0 for *M* = 5, and 65 are demonstrated in Figure 9(a) and (b), for *Da* = 0.01 and 0.1 respectively.

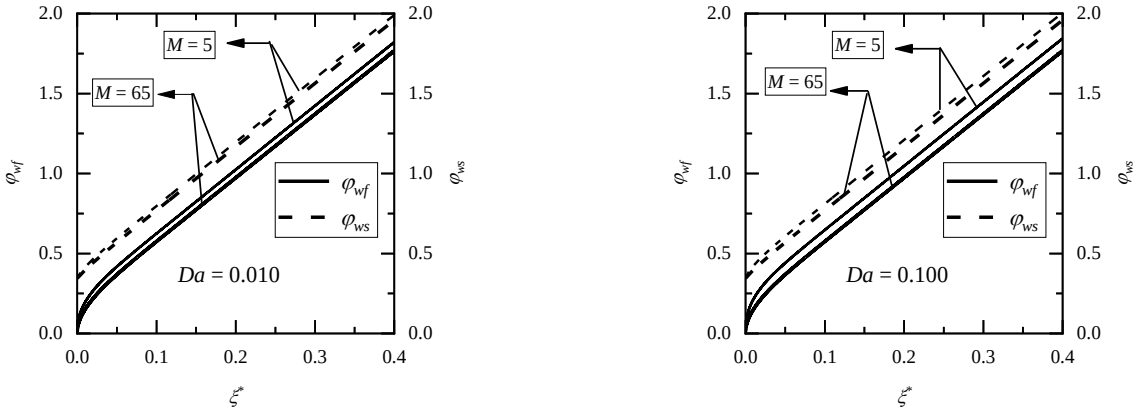

Fig. 9. Impact of φ_{wf} and φ_{ws} with ξ^* for *F* = 100, *Bi* = 10, and for *M* = 5, 65 and κ = 1.0 for (a) *Da* = 0.010 and (b) *Da* = 0.100

As ξ^* increases, wall temperatures in the fluid phase (φ_{wf}) and solid phase (φ_{ws}) also increase for all Hartman numbers. φ_{wf} and, φ_{ws} increase as ξ^* increases, initially non-linearly and then linearly for ξ^* > 0.03, say. This is the condition for the onset of a fully developed temperature field, where the constant heat flux is employed at the channel walls. From Figure 9, it can be observed that φ_{ws} > φ_{wf} because of the heat transmission from the fluid to the solid is more to solid wall temperature than the fluid wall temperature.

5.2.3 Local Nusselt number

The effect of the local Nusselt number Nu_ξ with ξ^* for *Bi* = 10, κ = 1.0 and *F* = 10 is shown in Figure 10(a) and (b) for (a) *Da* = 0.001 and (b) *Da* = 0.05 respectively for *M* = 1, 10, 25, 50, and 65. The variation of Nu_ξ with ξ^* for various values of Biot number for a given *Da* = 0.005, κ = 1.0, and *F* = 10 are given in Figure 11 for (a) *M* = 5, and (b) *M* = 65 respectively. Plots for the variation of Nu_ξ with ξ^* for various thermal conductivities (κ) are given in Figure 12 for low *Da* = 0.01 and Figure 13 for moderate *Da* = 0.05.

From Figure 10 to 13, Nu_ξ decreases with the increase of ξ^*. The trends in the variation of Nu_ξ with ξ^* for the channel coming under a porous medium are similar to the well-reported trend for the channel with clear fluid flow under the local thermal equilibrium.

From Figure 10(a) and (b), Nu_ξ increases with the increase of Hartman number, *M*. The same pattern is also seen in Figures 11 to 13 for small and large values of *M*. This fact is also observed in Figure 2(a)-(c) for the fully developed Nusselt number. In Figure 10, it can also be seen that as Darcy number, *Da* increases, Nu_ξ decreases and for large *Da* (say *Da* = 0.1), values of Nu_ξ for the channel with porous material are the same as values Nu_ξ for the clear fluid channel. At ξ^* = 0.4, values of Nu_ξ are the same as the fully developed Nusselt numbers (Nu_ξ) with different Hartman numbers, *M* at *Da* = 0.005, *F* = 0, *Bi* = 10, κ = 0.1 (as given in Table 1).

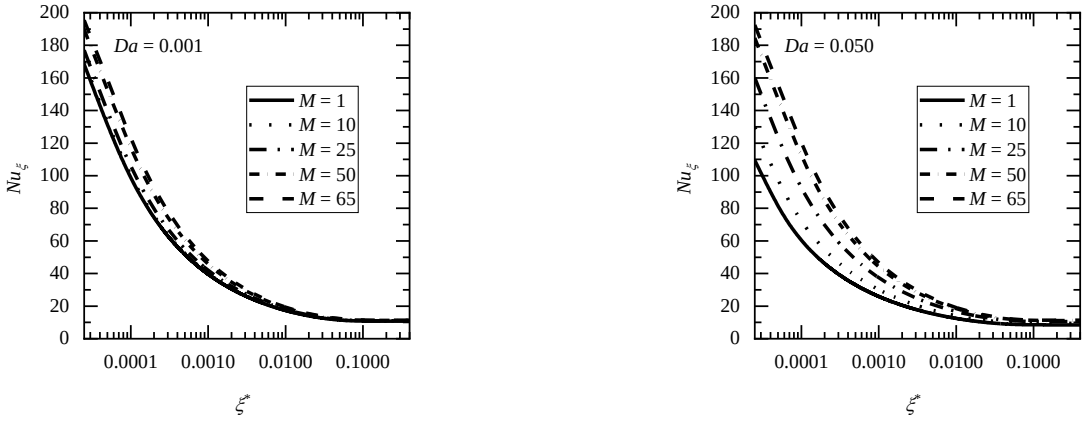

Fig. 10. Nu_{ξ} effect with ξ^* for distinct *M* values with *Bi* = 10, κ = 0.1, and *F* = 10 for (a) *Da* = 0.001 and (b) *Da* = 0.050

From Figure 11 to 13, there are significant changes in local Nusselt numbers with ξ^* for higher Biot numbers and, κ. This fact was reported by Dehghan *et al.*, [41]. From Figure 11(a) and (b), as the Biot number increases the local Nusselt number decreases for a given *Da*, *F*, *M*, and κ. This feature was observed for the constant wall temperature boundary condition and in the absence of the Hartman number given in Nield *et al.*, [42].

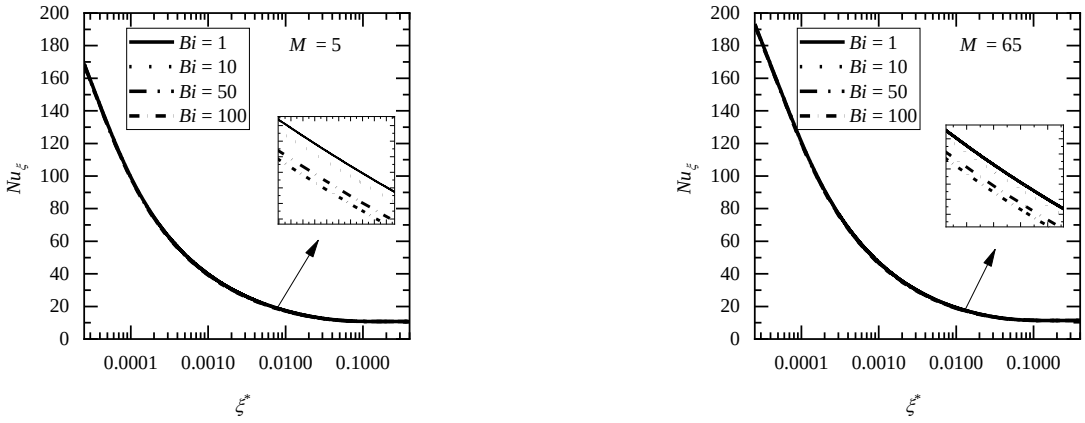

Fig. 11. Nu_{ξ} effect with ξ^* for distinct *Bi* values with *Da* = 0.005, κ = 0.1, and *F* = 10 for (a) *M* = 5 and (b) *M* = 65

From Figure 12 and 13, as κ increases from 0.1 to 10.0, Nu_{ξ} value decreases for all the values of the Hartman number, Biot number, Darcy number, and Forchheimer number. This fact is also given in Figure 2(a)-(c) for all the values of *M*. The value of Nu_{ξ} is less influenced by the Forchheimer number (*F*) for all the Hartman numbers, and Biot numbers. Nu_{ξ} increases, as the Forchheimer number increases, and the amount of decrease is smaller in quantity.

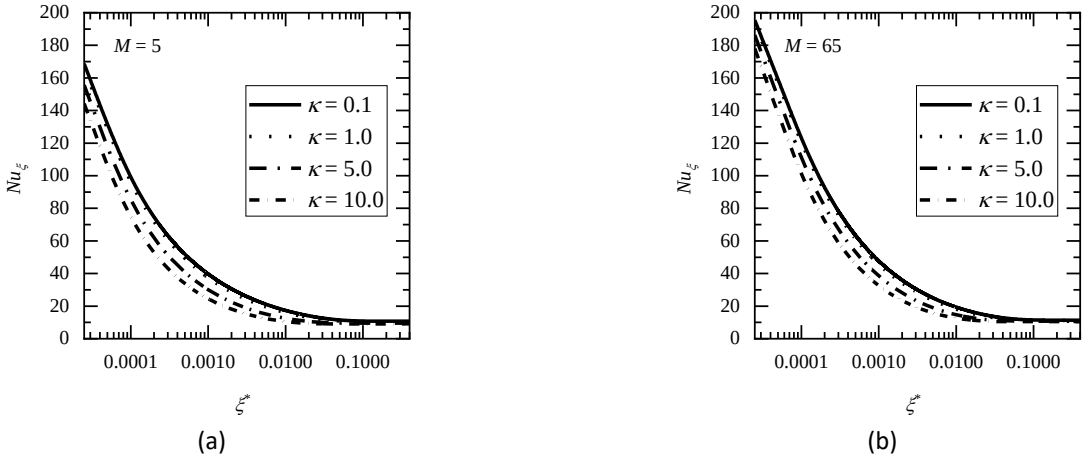

Fig. 12. Nu_ξ effect with ξ^* for distinct κ values with *Da* = 0.001, *Bi* = 10, and *F* = 10 for (a) *M* = 5 and (b) *M* = 65

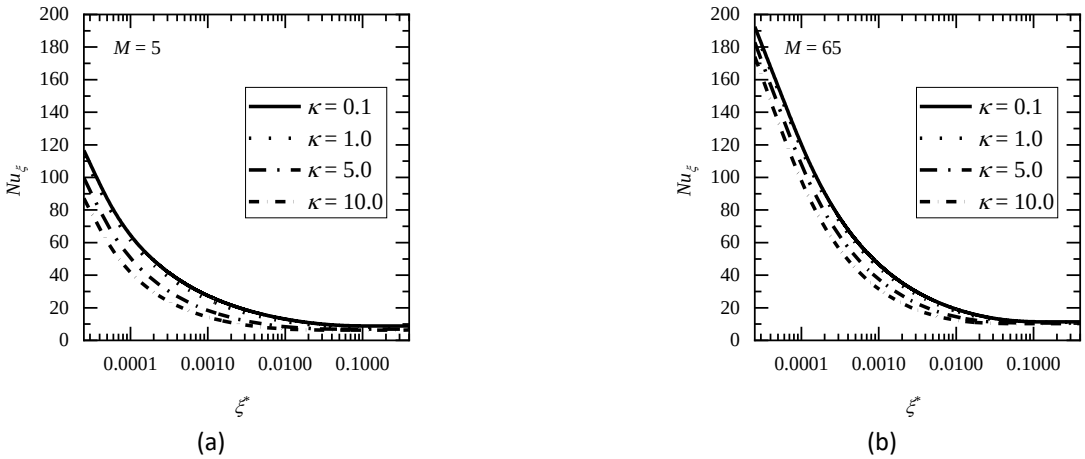

Fig. 13. Nu_ξ effect with ξ^* for distinct κ values with *Da* = 0.050, *Bi* = 10, and *F* = 10 for (a) *M* = 5 and (b) *M* = 65

At the fully developed length, say $\xi^* \geq 0.38$, local Nusselt numbers (Nu_ξ) approach to the fully developed Nusselt numbers, which are obtained analytically. Local Nusselt numbers, (Nu_ξ) at ξ^* = 0.38 and the fully developed Nusselt numbers values (Eq. (29)) are given in Table 1 for different Hartman numbers, M = 1, 5 and 10 for *Da* = 0.005, *F* = 0, *Bi* = 10, κ = 0.1. At the fully developed length, say $\xi^* > 0.38$, local Nusselt numbers (Nu_ξ) approach to the fully developed Nusselt numbers, Nu_{fd}, which are obtained analytically which can be seen in Table 1.

Table 1
Local Nusselt numbers (Nu_ξ), and the fully developed Nusselt numbers (Nu_{fd}) values with various Hartman numbers, *M*

M	Nu_ξ at ξ^* = 0.38	Nu_{fd}
1	9.753	9.894
5	9.832	9.971
10	10.143	9.165

The variation of Forchheimer number, *F* on Nu_ξ is given in Table 2 at various ξ^* at Darcy number, *Da* = 0.001, κ = 0.1, and at Hartman number, *M* = 5, and 65. From the Table 2, it clear that effect of *F* is very less on Nu_ξ may be because of the magnetic field effect.

Table 2
Variation of local Nusselt number, Nu_ξ for different Forchheimer number, *F*

	M = 5, *Bi* = 50			*M* = 65, *Bi* = 50		
ξ^*	*F* = 1	*F* = 10	*F* = 100	*F* = 1	*F* = 10	*F* = 100
0.00005	130.977	130.977	130.979	158.864	158.864	158.864
0.00010	98.670	98.670	98.672	122.599	122.599	122.599
0.00100	39.285	39.285	39.286	47.222	47.222	47.222
0.00500	21.744	21.744	21.744	24.806	24.806	24.806
0.05000	11.447	11.448	11.448	12.244	12.244	12.244

6. Comparison of Present Work with the Existing Literature

To validate the present work, the comparison between present values of local and fully developed Nusselt number with Gupta and Bhargavi [39] for *Bi* = 50, κ = 0.1, *F* = 100 in the absences of the magnetic field, *M* = 0 is given in Table 3. The agreement is very good.

Table 3
The comparison between present values of local and fully developed Nusselt number with Gupta and Bhargavi [39]

	Gupta and Bhargavi [39]		Present value	
Da	Nu_ξ	Nu_{fd}	Nu_ξ	Nu_{fd}
0.001	167.935	10.756	167.935	10.756
0.005	138.326	9.783	138.326	9.782
0.010	127.090	9.334	127.090	9.332
0.050	110.011	8.618	110.010	8.618
0.100	106.894	8.494	106.894	8.494

7. Conclusion

In this work, the numerical investigation of forced convective heat transfers in the thermal entry of parallel plate channels completely immersed in porous media under local thermal non-equilibrium circumstances is discussed. The parallel plates are exposed to a constant wall heat flux. The flow field is unidirectional and obeys the Darcy Brinkman Forchheimer equation. The problem was defined by Darcy number (*Da*), Hartman number (*M*), thermal conductivity ratio (κ), Biot number (*Bi*), and, Forchheimer coefficient (*F*). The numerical solution has been adduced for temperatures in both phases solid and fluid, wall temperature, and local Nusselt number at the entrance to the channel filled with porous medium for LTNE condition. The key findings on the behaviour of the investigated system are

i. For all the values of Hartman number, *M* and for the large *Bi*, φ_s is decreasing and tends to temperature in a fluid region under LTE. It means LTNE tends to LTE. when the Biot number large. Also, φ_s is larger than the temperature in a fluid phase φ_f. This is the validation of LTNE condition.

ii. As ξ^* increases, φ_{wf} and, φ_{ws} increase, initially non-linearly and then linearly for $\xi^* > 0.03$, say. This is the condition for the onset of a fully developed temperature field. Moreover, $\varphi_{ws} > \varphi_{wf}$ because heat transmission from fluid to solid is greater at solid wall temperature than fluid wall temperature.

iii. With the increase of Hartman number, *M*, local Nusselt number increases. This fact is also true for fully developed Nusselt number (as given in the figures).

iv. Local Nusselt number (Nu_ξ) value decreases with increase of *Da*. For large value of *Da* (say *Da* = 0.1), value of Nu_ξ for the channel with porous material is the same as value of Nu_ξ for the clear fluid channel.

v. For all the values of Hartman number, Nu_ξ decreases with increase of thermal conductivity ratio, *κ*. This fact is also true for fully developed Nusselt number.

Acknowledgement
One of the authors, Nitish Gupta thanks the MHRD Government of India for his Doctoral Scholarship.

References

[1] Sunhazim, Nur Shamimi Amirah Md, Ummi Aqila Norhaidi, Muhammad Afiq Witri Muhammad Yazid, Fazila Mohd Zawawi, and Ummikalsom Abidin. "Characterization of fluid flow through porous media." *Journal of Advanced Research in Fluid Mechanics and Thermal Sciences* 96, no. 2 (2022): 22-32. https://doi.org/10.37934/arfmts.96.2.2232

[2] Vafai, Kambiz, and Chang L. Tien. "Boundary and inertia effects on flow and heat transfer in porous media." *International Journal of Heat and Mass Transfer* 24, no. 2 (1981): 195-203. https://doi.org/10.1016/0017-9310(81)90027-2

[3] Nield, Donald A., and Adrian Bejan. *Convection in porous media*. Vol. 3. New York: springer, 2006.

[4] Nakayama, Akira. *PC-aided numerical heat transfer and convective flow*. CRC press, 1995.

[5] Amiri, A., and Kambiz Vafai. "Analysis of dispersion effects and non-thermal equilibrium, non-Darcian, variable porosity incompressible flow through porous media." *International journal of heat and mass transfer* 37, no. 6 (1994): 939-954. https://doi.org/10.1016/0017-9310(94)90219-4

[6] Carbonell, Ruben G., and Stephen Whitaker. "Heat and mass transfer in porous media." *Fundamentals of transport phenomena in porous media* (1984): 121-198. https://doi.org/10.1007/978-94-009-6175-3_3

[7] Fichot, Florian, Fabien Duval, Nicolas Tregoures, C. Béchaud, and Michel Quintard. "The impact of thermal non-equilibrium and large-scale 2D/3D effects on debris bed reflooding and coolability." *Nuclear engineering and design* 236, no. 19-21 (2006): 2144-2163. https://doi.org/10.1016/j.nucengdes.2006.03.059

[8] Kuznetsov, A. V., and D. A. Nield. "Effect of local thermal non-equilibrium on the onset of convection in a porous medium layer saturated by a nanofluid." *Transport in Porous Media* 83 (2010): 425-436. https://doi.org/10.1007/s11242-009-9452-8

[9] Straughan, B. "Green–Naghdi fluid with non-thermal equilibrium effects." *Proceedings of the Royal Society A: Mathematical, Physical and Engineering Sciences* 466, no. 2119 (2010): 2021-2032. https://doi.org/10.1098/rspa.2009.0523

[10] Zhang, W., X. Bai, M. Bao, and A. Nakayama. "Heat transfer performance evaluation based on local thermal non-equilibrium for air forced convection in channels filled with metal foam and spherical particles." *Applied Thermal Engineering* 145 (2018): 735-742. https://doi.org/10.1016/j.applthermaleng.2018.09.097

[11] Zhang, Shikun, Zhongwei Huang, Haizhu Wang, Hongyuan Zhang, Chengcheng Zhang, and Chao Xiong. "Thermal characteristics analysis with local thermal non-equilibrium model during liquid nitrogen jet fracturing for HDR reservoirs." *Applied Thermal Engineering* 143 (2018): 482-492. https://doi.org/10.1016/j.applthermaleng.2018.07.088

[12] Li, Xiaoya, Yan Li, Pengfei Luo, and Xiaogeng Tian. "Relationship between the nonlocal effect and lagging behavior in bioheat transfer." *Journal of Heat Transfer* 143, no. 5 (2021). https://doi.org/10.1115/1.4049997

[13] Kuznetsov, A. V., and D. A. Nield. "Local thermal non-equilibrium effects on the onset of convection in an internally heated layered porous medium with vertical throughflow." *International Journal of Thermal Sciences* 92 (2015): 97-105. https://doi.org/10.1016/j.ijthermalsci.2015.01.019

[14] Yi, Yuan, Xiaohui Bai, Fujio Kuwahara, and Akira Nakayama. "Analytical and numerical study on thermally developing forced convective flow in a channel filled with a highly porous medium under local thermal non-equilibrium." *Transport in Porous Media* 136 (2021): 541-567. https://doi.org/10.1007/s11242-020-01524-8
[15] Yi, Yuan, Xiaohui Bai, Fujio Kuwahara, and Akira Nakayama. "A Local Thermal Non-Equilibrium Solution Based on the Brinkman–Forchheimer-Extended Darcy Model for Thermally and Hydrodynamically Fully Developed Flow in a Channel Filled With a Porous Medium." *Transport in Porous Media* 139 (2021): 67-88. https://doi.org/10.1007/s11242-021-01645-8
[16] Lee, Dae-Young, and Kambiz Vafai. "Analytical characterization and conceptual assessment of solid and fluid temperature differentials in porous media." *International Journal of Heat and Mass Transfer* 42, no. 3 (1999): 423-435. https://doi.org/10.1016/S0017-9310(98)00185-9
[17] Amiri, A., K. Vafai, and T. M. Kuzay. "Effects of boundary conditions on non-Darcian heat transfer through porous media and experimental comparisons." *Numerical Heat Transfer, Part A: Applications* 27, no. 6 (1995): 651-664. https://doi.org/10.1080/10407789508913724
[18] Marafie, A., and K. Vafai. "Analysis of non-Darcian effects on temperature differentials in porous media." *International Journal of Heat and Mass Transfer* 44, no. 23 (2001): 4401-4411. https://doi.org/10.1016/S0017-9310(01)00099-0
[19] Singh, Chanpreet, R. G. Tathgir, and K. Muralidhar. "Experimental validation of heat transfer models for flow through a porous medium." *Heat and mass transfer* 43 (2006): 55-72. https://doi.org/10.1007/s00231-006-0091-0
[20] Sreekala, L., and E. Kesava Reddy. "Steady MHD Couette flow of an incompressible viscous fluid through a porous medium between two infinite parallel plates under effect of inclined magnetic field." *The International Journal of Engineering and Science (IJES)* 3, no. 9 (2014): 18-37.
[21] Kiema, D. W., W. A. Manyonge, J. K. Bitok, R. K. Adenyah, and J. S. Barasa. "On the steady MHD couette flow between two infinite parallel plates in an uniform transverse magnetic field." (2015).
[22] Chauhan, D. S., and Priyanka Rastogi. "Heat transfer and entropy generation in MHD flow through a porous medium past a stretching sheet." *Int. J. Energ. Tech* 3 (2011): 1-13.
[23] Onyango, Edward Richard, Mathew Ngugi Kinyanjui, and Surindar Mohan Uppal. "Unsteady hydromagnetic Couette flow with magnetic field lines fixed relative to the moving upper plate." *American Journal of Applied Mathematics* 3, no. 5 (2015): 206-214. https://doi.org/10.11648/j.ajam.20150305.11
[24] Raju, K. V. S., T. Sudhakar Reddy, M. C. Raju, PV Satya Narayana, and S. Venkataramana. "MHD convective flow through porous medium in a horizontal channel with insulated and impermeable bottom wall in the presence of viscous dissipation and Joule heating." *Ain Shams Engineering Journal* 5, no. 2 (2014): 543-551. https://doi.org/10.1016/j.asej.2013.10.007
[25] Verma, Vineet Kumar, and Amit Kumar Gupta. "Analytical Solution of the Flow in a Composite Cylindrical Channel Partially Filled with a Porous Medium in the Presence of Magnetic Field." *Special Topics & Reviews in Porous Media: An International Journal* 8, no. 1 (2017). https://doi.org/10.1615/SpecialTopicsRevPorousMedia.v8.i1.30
[26] Kurzweg, Ulrich H. "The stability of Couette flow in the presence of an axial magnetic field." *Journal of Fluid Mechanics* 17, no. 1 (1963): 52-60. https://doi.org/10.1017/S0022112063001099
[27] Raptis, A. A., and C. P. Pfrdikis. "Combined free and forced convection flow through a porous medium." *International Journal of Energy Research* 12, no. 3 (1988): 557-560. https://doi.org/10.1002/er.4440120319
[28] Bhargavi, D., and J. Sharath Kumar Reddy. "Analytical study of forced convection in a channel partially filled with porous material with effect of magnetic field: constant wall heat flux." *Special Topics & Reviews in Porous Media: An International Journal* 9, no. 3 (2018). https://doi.org/10.1615/SpecialTopicsRevPorousMedia.v9.i3.10
[29] Pal, Dulal. "Magnetohydrodynamic non-Darcy mixed convection heat transfer from a vertical heated plate embedded in a porous medium with variable porosity." *Communications in Nonlinear Science and Numerical Simulation* 15, no. 12 (2010): 3974-3987. https://doi.org/10.1016/j.cnsns.2010.02.003
[30] Vafai, K., and SJin Kim. "On the limitations of the Brinkman-Forchheimer-extended Darcy equation." *International Journal of Heat and Fluid Flow* 16, no. 1 (1995): 11-15. https://doi.org/10.1016/0142-727X(94)00002-T
[31] Maghrebi, Mohammad Javad, M. Nazari, and T. Armaghani. "Forced convection heat transfer of nanofluids in a porous channel." *Transport in porous media* 93 (2012): 401-413. https://doi.org/10.1007/s11242-012-9959-2
[32] Vaidya, H., C. Rajashekhar, K. V. Prasad, S. U. Khan, F. Mebarek-Oudina, A. Patil, and P. Nagathan. "Channel flow of MHD bingham fluid due to peristalsis with multiple chemical reactions: an application to blood flow through narrow arteries." *SN Applied Sciences* 3 (2021): 1-12. https://doi.org/10.1007/s42452-021-04143-0
[33] Hanafi, Hajar, and Sharidan Shafie. "Unsteady free convection MHD flow over a vertical cone in porous media with variable heat and mass flux in presence of chemical reaction." *Journal of Advanced Research in Fluid Mechanics and Thermal Sciences* 92, no. 2 (2022): 1-12. https://doi.org/10.37934/arfmts.92.2.112

[34] Balachandra, H., Choudhari Rajashekhar, Hanumesh Vaidya, Fateh Mebarek Oudina, Gudekote Manjunatha, and Kerehalli Vinayaka Prasad. "Homogeneous and heterogeneous reactions on the peristalsis of bingham fluid with variable fluid properties through a porous channel." *Journal of Advanced Research in Fluid Mechanics and Thermal Sciences* 88, no. 3 (2021): 1-19. https://doi.org/10.37934/arfmts.88.3.119

[35] Divya, B. B., G. Manjunatha, C. Rajashekhar, Hanumesh Vaidya, and K. V. Prasad. "Analysis of temperature dependent properties of a peristaltic MHD flow in a non-uniform channel: a Casson fluid model." *Ain Shams Engineering Journal* 12, no. 2 (2021): 2181-2191. https://doi.org/10.1016/j.asej.2020.11.010

[36] Zokri, Syazwani Mohd, Nur Syamilah Arifin, Abdul Rahman Mohd Kasim, Norhaslinda Zullpakkal, and Mohd Zuki Salleh. "Forced Convection of MHD Radiative Jeffrey Nanofluid Over a Moving Plate." *Journal of Advanced Research in Fluid Mechanics and Thermal Sciences* 87, no. 1 (2021): 12-19. https://doi.org/10.37934/arfmts.87.1.1219

[37] Douha, Mohammed, Draoui Belkacem, Kaid Noureddine, Ameur Houari, Belkacem Abdellah, Mohamed Elmir, Merabti Abdelhak, and Aissani Houcine. "Study of laminar naturel convection in partially porous cavity in the presence of nanofluids." *Journal of Advanced Research in Fluid Mechanics and Thermal Sciences* 79, no. 1 (2020): 91-110. https://doi.org/10.37934/arfmts.79.1.91110

[38] Reddy, J. Sharath Kumar, and D. Bhargavi. "NUMERICAL STUDY OF FLUID FLOW IN A CHANNEL PARTIALLY FILLED WITH POROUS MEDIUM WITH DARCY− BRINKMAN− FORCHHEIMER EQUATION." *Special Topics & Reviews in Porous Media: An International Journal* 9, no. 4 (2018). https://doi.org/10.1615/SpecialTopicsRevPorousMedia.2018022123

[39] Bhargavi, Nitish Guptaand D. "NUMERICAL INVESTIGATION OF HEAT TRANSFER IN A DEVELOPING THERMAL FIELD IN THE POROUS-FILLED DUCT UNDER LOCAL THERMAL NON-EQUILIBRIUM: CONSTANT WALL HEAT FLUX." (2022).

[40] Bhargavi, D., and J. Sharath Kumar Reddy. "Effect of heat transfer in the thermally developing region of the channel partially filled with a porous medium: constant wall heat flux." *International Journal of Thermal Sciences* 130 (2018): 484-495. https://doi.org/10.1016/j.ijthermalsci.2018.04.039

[41] Dehghan, Maziar, Mohammad Sadegh Valipour, Seyfolah Saedodin, and Yasser Mahmoudi. "Thermally developing flow inside a porous-filled channel in the presence of internal heat generation under local thermal non-equilibrium condition: a perturbation analysis." *Applied Thermal Engineering* 98 (2016): 827-834. https://doi.org/10.1016/j.applthermaleng.2015.12.133

[42] Nield, D. A., A. V. Kuznetsov, and Ming Xiong. "Effect of local thermal non-equilibrium on thermally developing forced convection in a porous medium." *International Journal of Heat and Mass Transfer* 45, no. 25 (2002): 4949-4955. https://doi.org/10.1016/S0017-9310(02)00203-X